First-principles interatomic potentials for transition-metal aluminides. II. Application to Al-Co and Al-Ni phase diagrams

Mike Widom
Department of Physics, Carnegie Mellon University, Pittsburgh, Pennsylvania 15213

John A. Moriarty
Lawrence Livermore National Laboratory, University of California, Livermore, California 94551
(Received 8 May 1998)

Aluminum-rich intermetallic compounds and alloys are important for their technological applications and scientifically interesting for their complex structures such as quasicrystals. Detailed knowledge of interatomic interactions can help explain structural and mechanical properties of these systems. The first paper of this series [Phys. Rev. B **56**, 7905 (1997)] derived first-principles interatomic potentials for alloys of aluminum with first row transition metals from generalized pseudopotential theory (GPT). This paper assesses the ability of those potentials to reproduce and elucidate the binary alloy phase diagrams of $Al_{1-x}Co_x$ and $Al_{1-x}Ni_x$. When the full theory is taken into account, we successfully reproduce the phase diagrams up to $x=0.3$. While many of the general features of the phase diagrams can be obtained with $x=0$ GPT pair potentials alone, the volume and composition dependence of the total energy become important by $x=0.25$. In addition, for certain complex structures, we introduce partial aluminum occupancy and demonstrate its importance. At high transition-metal concentration $x>0.25$, we must further include three- and four-body transition-metal interactions to account for the stability of Al_5Co_2 in the $Al_{1-x}Co_x$ phase diagram. [S0163-1829(98)06538-2]

I. INTRODUCTION

Highly stable Al-Ni-Co magnets, low thermal expansion invar (Ni_3Fe) and high-strength Ni-based superalloys prove the importance of intermetallic compounds.[1] Aluminum-based intermetallics boast high-strength/high-temperature and oxidation-resistant compounds such as Ni-Al, Fe-Al and Ti-Al.[2] In addition to their technologically useful properties, intermetallics also exhibit scientifically interesting complex structures.[3] Noteworthy among these alloys are quasicrystals, ordered structures displaying crystallographically forbidden icosahedral or decagonal symmetry.[4] Thus both technological need and fundamental scientific interest motivate study of these systems.

To explain their unusual structures and mechanical properties, we study atomic cohesion in intermetallic compounds. A previous paper[5] (henceforth referred to as paper I) established a first-principles generalized pseudopotential theory (GPT) for the total energy of aluminum-rich binary alloys with first-row transition-metal (TM) elements in terms of real-space interatomic potentials. To further assess the accuracy and dependability of that calculational approach, this paper applies the GPT to an in depth study of mechanical and thermodynamic stability over a range of composition in Al-Co and Al-Ni systems. Mechanical stability for a given structure reflects energy-minimizing atomic displacements to an equilibrium configuration under static relaxation at fixed composition and fixed volume or pressure. Thermodynamic stability demands that the final equilibrium structure lies on the convex hull of a graph of total energy per atom versus composition for all conceivable structures. This means the total energy would increase if a given structure were to decompose into a mixture of other phases of differing composition. Requiring mechanical and thermodynamic stability of known phases, and thermodynamic instability of hypothetical structures, is a stringent test of the interatomic potentials.

This paper considers aluminum-rich intermetallics of composition $Al_{1-x}TM_x$ with $x<0.3$. The electronic structure of these intermetallic alloys is complicated because aluminum contains weakly bound *s*- and *p*-band valence electrons, while transition metals have in addition tightly bound *d*-band electrons at, or near, the Fermi surface. A useful theory of interatomic interactions must correctly account for and link these electronic states. In the GPT this is accomplished by using a mixed basis of plane waves and localized TM *d* states and isolating weak *sp* pseudopotential, *sp*-*d* hybridization, and *d*-*d* tight-binding matrix elements. One then employs a rigorous expansion of the electron density and total energy in terms of these matrix elements and develops a real-space total-energy functional as a collective volume term plus sums over two-, three-, and higher-body interactions.[5,6] Because of its weak *sp* electron-ion pseudopotential, the pure aluminum total energy may be reasonably well approximated by a structure-independent volume term plus a pairwise sum over a two-ion interatomic potential. Transition metal *d*-band electrons also create strong angle-dependent three- and higher-body interactions. Because the *d*-orbitals are strongly localized in the vicinity of transition metal ions, significant contributions to the total energy from these many-body interactions are expected primarily when TM atoms have two or more TM neighbors. Such TM clusters are common at large TM concentration *x* but are rare for $x\ll 1$. Consequently, for $x<0.3$ the structural energetics are dominated by the two-ion pair contributions.

Paper I developed $Al_{1-x}TM_x$ GPT interatomic potentials and applied them to study cohesive and structural trends among binary alloys of aluminum with transition metals across the $3d$ series. This paper focuses on a more thorough

TABLE I. Structural data for real and hypothetical Al-Co and Al-Ni phases up to $x=0.3333$.

Name	Pearson symbol (Strukturebericht)	Space group	Reference	x
FCC	$cF4$ ($A1$)	$Fm\bar{3}m$	25	0.0000
HCP	$hP2$ ($A3$)	$P6_3/mmc$	25	0.0000
BCC	$cI2$ ($A2$)	$Im3m$	25	0.0000
$Al_{12}W$	$cI26$	$Im3$	25	0.0769
Al_6Mn	$oC28$ ($D2_h$)	$Cmcm$	25	0.1429
Al_9Co_2	mP22	$P2_1/a$	25	0.1818
Al_4Mn	oP156	$Pn2_1a$	36	0.2051
$Al_{10}Mn_3$	$hP26$	$P6_3/mmc$	25	0.2308
M-$Al_{13}Co_4$	$mC102$	$C2/m$	13	0.2353+
O-$Al_{13}Co_4$	$oP102$	$Pmn2_1$	22	0.2353+
$Al_{75}Co_{22}Ni_3$	$mC34$-1.8	$C2/m$	15	0.2480
W_3O	$cP8$ ($A15$)	$Pm3n$	25	0.2500
$AuCu_3$	$cP4$ ($L1_2$)	$Pm3m$	25	0.2500
Fe_3Al	$cF16$ ($D0_3$)	$Fm3m$	25	0.2500
Al_3Ti	$tI8$ ($D0_{22}$)	$I4/mmm$	25	0.2500
Al_3Ni	$oP16$ ($D0_{11}$)	$Pnma$	25	0.2500
$Al_{11}Mn_4$	$aP15$	$P\bar{1}$	25	0.2667
$Al_{11}Co_4$	$mP52$	$P2$	16	0.2692
Al_5Co_2	$hP28$	$P6_3/mmc$	25	0.2857
Al_5Fe_2	$oC16$	$Cmcm$	25	0.2857
Al_3Mn	$oP160$	$Pnma$	35	0.3077
Al_2Cu	$tI12$ (C16)	$I4/mcm$	25	0.3333
CaF_2	$cF12$ (C1)	$Fm3m$	25	0.3333

evaluation of the potentials and their ability to reproduce complicated phase diagrams. Our measures of success are, first, whether known structures possess mechanical stability under relaxation, and second, whether we can reproduce the known equilibrium phase diagrams.

We focus on binary alloys of aluminum with cobalt and with nickel. This choice is motivated by several factors: (1) Preexisting pair potentials for the $Al_{1-x}Co_x$ alloys calculated by Phillips *et al.*,[7], which were also applied to the Al-Co phase diagram. These potentials were developed from a similar but simplified perturbative method, which neglected, among other things, direct *d-d* interactions and treated explicitly only the limit $x\rightarrow 0$. (2) Remaining uncertainties in the details of the Al-Co phase diagram, especially in the vicinity of $x=0.25$. (3) The chance to test the sensitivity of structural energies to a minimal shift in chemistry between neighboring transition metals. In particular, Al-Co and Al-Ni compounds exhibit somewhat different stable structures. (4) Our future intention is to extend the binary-alloy potentials to the ternary compound Al-Ni-Co. This ternary compound possesses a thermodynamically stable decagonal quasicrystal phase.[8]

The following section of this paper presents the experimentally determined Al-Co and Al-Ni binary alloy phase diagrams. We describe crystal structures of special interest, and compare the phase diagrams and crystal structures between the two alloys families. Section III reviews the GPT total energy and interatomic potentials. We show how the long-range Friedel oscillations of the pair potentials correlate with structural features of stable crystals. These potentials are then applied to the phase diagrams at different levels of approximation. Our baseline approach follows Phillips *et al.*[7] and assumes a constant electron density, ignoring the actual concentration dependence of the total energy. Calculational results obtained with this approach up to $x=0.3$ are presented in Sec. IV A and use only pair potentials evaluated in the $x\rightarrow 0$ limit. The advantage of this approach is that one can easily consider a range of composition without recalculating the potentials. Also, pair potentials are convenient for static relaxation and other computer simulation methods. However, this approach is not rigorously valid and will even-

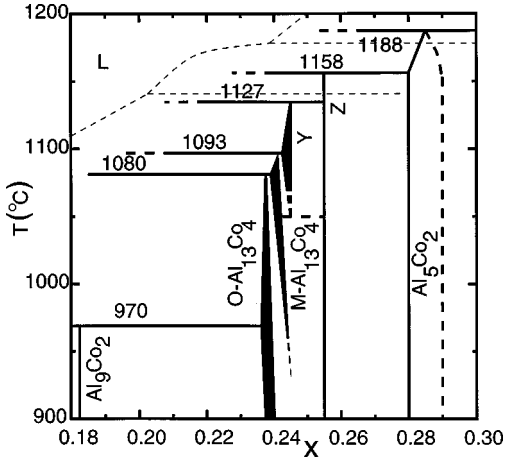

FIG. 1. Phase diagram of $Al_{1-x}Co_x$ near composition Al_3Co adapted from Grushko *et al.* (Ref. 11).

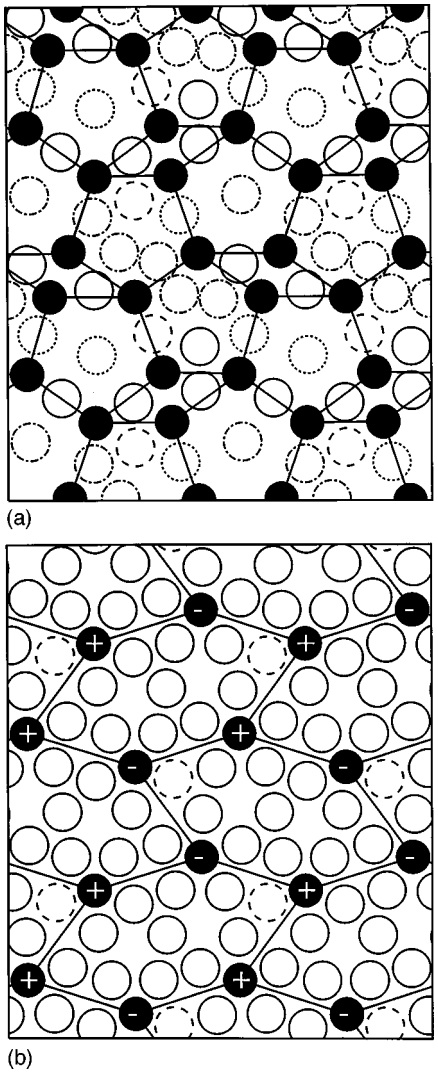

FIG. 2. Structure of O-$Al_{13}Co_4$ as determined by Grin *et al.* (Ref. 22). (a) Flat F layer. (b) Puckered P layer. Black disks denote Co atoms. White circles denote Al atoms. See text (Sec. IV B) for explanation of dashed and dotted Al atoms. Four unit cells (2×2) are shown.

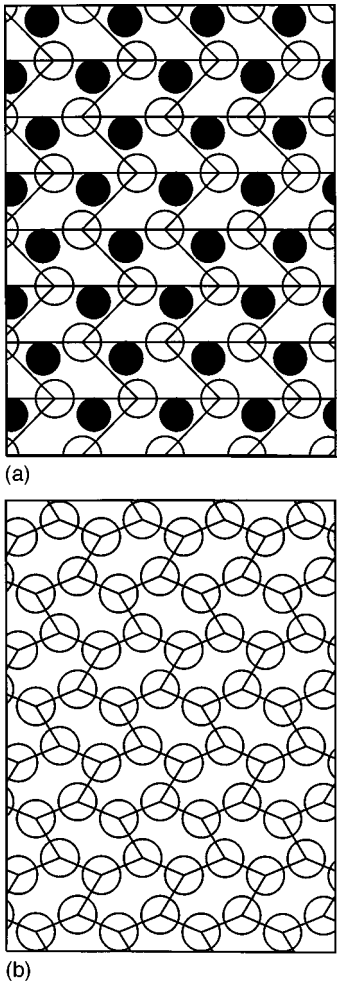

FIG. 3. Structure of Al_3Ni. (a) Flat F layer. (b) Puckered P layer. Black disks denote Ni atoms. White circles denote Al atoms. Sixteen unit cells (4×4) are shown.

tually break down for sufficiently large x. Our results show that the composition-dependence of the volume term and pair potentials is needed by $x=0.25$ and that many-body interactions play a crucial role by $x=0.2857$.

Detailed discussion of specific difficulties encountered in Sec. IV A, and their resolutions, is contained in the later subsections. We address the problem of partial occupancy, which is common among some aluminum sites in complex Al-Co structures, in Sec. IV B. Section IV C addresses the role of the volume- and composition-dependence of the potentials. Stability of Al-Co in the observed structure Al_5Co_2 against the competing structure of Al_5Fe_2 demands consideration of three- and four-body interactions, as we show in Sec. IV D. Finally, Sec. V summarizes our main conclusions.

II. AL-CO AND AL-NI PHASE DIAGRAMS

The Al-Co and Al-Ni phase diagrams and stable structures[9,10] differ markedly from each other, despite the fact that Co and Ni are neighboring transition metals in the Periodic Table. The observed Al-Co and Al-Ni structures, as well as many other candidate structures, are listed in Table I up to transition-metal fraction $x=0.3333$.

Details of the Al-Co phase diagram remain in doubt, especially in the vicinity of composition Al_3Co. Figure 1 illustrates the current evaluation of thermodynamic and structural data[11] near composition Al_3Co. Most of the phases are stable only at high temperatures, in accordance with the usual rule that phases nearby in composition cannot coexist over a wide range of temperature.[12] The orthorhombic phase O-$Al_{13}Co_4$ replaces the previously identified[9] monoclinic phase M-$Al_{13}Co_4$ as the thermodynamically stable variant. Trace impurities are required to stabilize the monoclinic form at low temperatures.[11] Furthermore, the space group of this monoclinic phase is identified as C2/m,[13] in contrast with the earlier claim of Cm.[14] The Y phase is believed related to $Al_{75}Co_{22}Ni_3$ which is homeotypical[15] to $Al_{13}Os_4$. There is, however, an alternate proposed structure for this phase known as $Al_{11}Co_4$.[16] The Z phase is also known as τ^2-$Al_{13}Co_4$ because its lattice constants are related approximately to those of M-$Al_{13}Co_4$ by two factors of the golden mean

$$\tau=\frac{\sqrt{5}+1}{2}. \tag{1}$$

Its precise structure is presently unknown.[17] In addition to the large number of stable crystalline phases, a metastable decagonal quasicrystal phases forms throughout this composition range.[18]

In contrast, the Al-Ni phase diagram contains relatively few and well understood structures. In the composition range of interest there is only one stable compound, Al_3Ni.

The cluster of phases near Al_3Co share common structural features. They may be described as layered structures, alternating flat and puckered layers. The spacing between layers is close to 2 Å, so the stacking repeat distance is about 8 Å. F is a flat mirror plane, while P is a puckered layer, with atoms displaced up to 0.34 Å above or below the mean height. P', the mirror image of P through F, is distinguished from P only through the sign of the puckering displacements. F' is equivalent to F after a translation perpendicular to the layering direction. The entire stacking sequence may be represented $FPF'P'$. The only exception to this rule, the Y phase, has a 4 Å repeat length. This is accommodated in $Al_{75}Co_{22}Ni_3$ by alternating a pair of F layers. In contrast, $Al_{11}Co_4$, alternates F and P type layers.[16] As a consequence, F cannot be a mirror plane, and is itself very slightly puckered in $Al_{11}Co_4$.

Another motif shared among these structures is a characteristic cluster of atoms known as a pentagonal bipyramid (PB).[19–21] This cluster is centered on a flat layer and extends to the adjacent puckered layers above and below. On the equator it features a pentagon of Co atoms (edge length 4.7 Å) centered by a single Al atom. It is capped in the puckered layers by a smaller pentagon of Al atoms (edge length 2.9 Å) centered by a single Co atom. Additional Al atoms occupy variable positions within the flat layers. Formation of the pentagonal bipyramid as a favored structure follows from highly advantageous interatomic bond lengths both within individual PB's and between neighboring PB's.[20]

Figure 2 illustrates the structure[22–24] of O-$Al_{13}Co_4$. Pentagonal motifs are clearly visible in both the flat and puckered layers. Structures of this type are known as decagonal quasicrystal approximants, because they employ structural elements believed to be similar to those of the decagonal quasicrystal phase, but repeated periodically in space. Lattice constants of different approximants ideally differ by powers of τ. For the so-called h/k-orthorhombic approximant the ideal lattice constants near composition Al_3Co take the values $a(h/k)=5.532\tau^h$, $b(h/k)=2.908\tau^k$, $c=8.12$ in units of angstroms.[21] The ideal lattice constants $a(2/3)=14.483$, $b(2/3)=12.318$ and $c=8.12$ are close to the experimentally observed ones of O-$Al_{13}Co_4$ (14.452 Å, 12.342 Å, and 8.158 Å). Hence we identify this structure as a 2/3 orthorhombic approximant.

The layering and some atomic motifs that are so common among Al_3Co structures are also present in Al_3Ni. This compound features the cementite ($D0_{11}$) structure illustrated in Fig. 3. Based on the layered structure, atomic motifs and lattice constants, Al_3Ni may be identified as a 0/1 orthorhombic approximant. The ideal lattice constants $a(0/1)=5.532$, $b(0/1)=4.706$ and $c=8.12$ are now rather far from the observed ones of the $D0_{11}$ structure illustrated in Fig. 3 (6.598, 4.802, and 7.351) because of the low order of approximant, and our use of ideal lattice constants devised for Al-Co compounds. The structural link among Al_3Ni and the Al_3Co phases places these structures in contention with each other for thermodynamic stability with slight shifts in stoichiometry and chemical composition interchanging relative stability.

At larger transition-metal content, $x=0.4$, Al_3Ni_2 has a simple structure with only 5 atoms per unit cell that has no known structural relation to AlCo compounds. At $x=0.5$, both Al-Co and Al-Ni take the simple CsCl (B2) structure.

III. INTERATOMIC POTENTIALS

Paper I described the theoretical basis for calculating interatomic potentials within the generalized pseudopotential theory (GPT). Here, we review some key ideas. The GPT interatomic potentials are terms in a real-space expansion of total energy in the form of volume, pair and many-body interactions:

$$E_{\rm tot}(\mathbf{R}_1\ldots\mathbf{R}_N)=NE_{\rm vol}(\Omega,x)+\frac{1}{2}\sum_{\alpha,\beta=A,B}\sum_{i,j}{}'\,v_2^{\alpha\beta}(R_{ij};\Omega,x)+\frac{1}{6}\sum_{\alpha,\beta,\gamma=A,B}\sum_{i,j,k}{}'\,v_3^{\alpha\beta\gamma}(R_{ij},R_{jk},R_{ki};\Omega,x)$$
$$+\frac{1}{24}\sum_{\alpha,\beta,\gamma,\delta=A,B}\sum_{i,j,k,l}{}'\,v_4^{\alpha\beta\gamma\delta}(R_{ij},R_{jk},R_{kl},R_{ik},R_{jl},R_{il};\Omega,x)+\cdots. \tag{2}$$

Here $\mathbf{R}_1\ldots\mathbf{R}_N$ denotes the positions on the N ions in the metal, Ω is the atomic volume, x the atomic composition, and the prime on each sum over ion positions excludes all self-interaction terms. A and B denote the two chemical species, Al and TM.

The volume term is structure independent. It exerts no force on the individual atoms, but is important for determining the cohesive energy, equilibrium volume, and bulk modulus. The pair-potential sums are the leading structure-dependent terms in the total energy. In general, both the pair and many-body potentials are long-ranged with oscillatory tails arising from electron screening and/or sp-d hybridization. The many-body interactions are presumed to be strongest among clusters of transition-metal atoms and weaker among clusters containing aluminum atoms. Consequently, the many-body interactions should be negligible at low

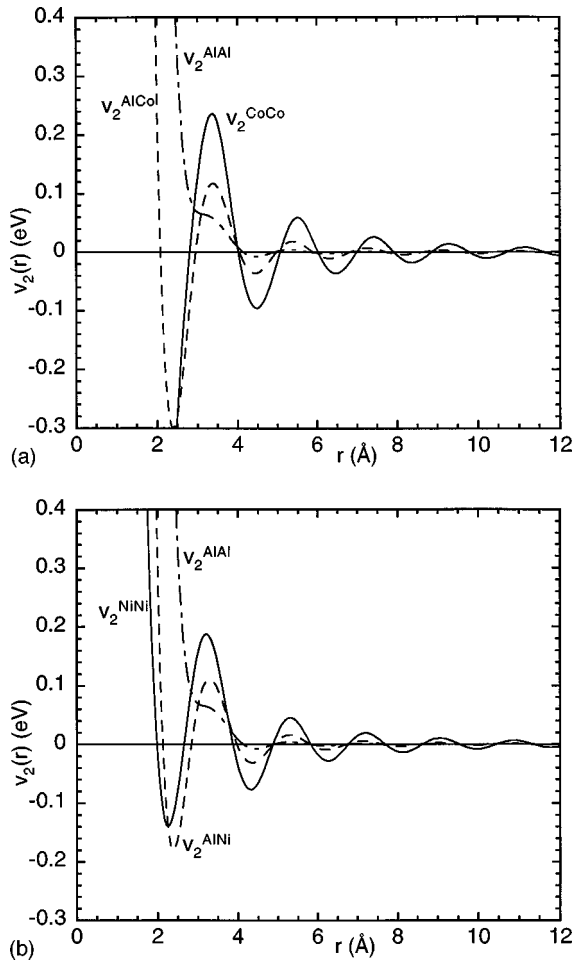

FIG. 4. GPT interatomic pair potentials at composition $x=0.25$ for (a) Al_3Co and (b) Al_3Ni. Dashed-dotted lines v_2^{AlAl}; dashed lines v_2^{AlTM}; solid lines v_2^{TMTM}.

transition-metal concentration, and grow progressively more important at higher transition-metal concentration. In pure elemental transition metals, the three- and four-body interactions are important, but higher-order interactions may often be neglected.

All terms in the GPT total-energy expansion depend on the atomic volume and chemical composition. The discussion in the following section compares use of GPT potentials evaluated in the $x\rightarrow 0$ limit with use of the full composition-dependent GPT potentials. Use of the $x=0$ potentials is motivated by the observation[7] that the valence electron density varies slowly with x, near $x=0$, for Al-Co compounds. We confirm in Sec. IV A that the $x=0$ potentials achieve considerable success, but find in Sec. IV C that the appearance of certain phases in the alloy phase diagrams requires the composition-dependent GPT.

Figure 4 displays the present GPT pair potentials evaluated at composition $x=0.25$. For Al_3Ni the potentials are evaluated at the experimental atomic volume of 98.24 a.u. For Al_3Co we use atomic volume 100.0 a.u., chosen because it is a round number interpolated between experimental atomic volumes of neighboring structures. Friedel-like oscillations with asymptotic wavelength related to the Fermi wave number are a characteristic feature of the pair potentials. The precise shapes of the GPT potentials vary slowly with x, as was discussed in paper I. The primary difference between the two sets of potentials is the relatively weak attractive TM-TM interactions at short range in Ni compared with those in Co. We can trace this difference back to the more nearly filled d-bands of Ni. The positions of potential minima and maxima are quite similar in the two compounds. Minima of the Ni-Ni potential are shifted slightly to the left of minima of the Co-Co potential, reflecting the growing nuclear charge and shrinking equilibrium volume in moving to the right in the $3d$ series and consistent with the trends noted in paper I.

Note the strongly negative Co-Co potential below $r=2.5$ Å. This indicates an unphysical overbinding of transition-metal ions caused by strongly attractive two-ion d-d interactions. They are offset in the bulk metal by corresponding repulsive many-body interactions. Their presence, however, serves as a warning of the limitations of a pair-potential treatment of the alloy. Provided TM ions remain well separated, our calculations are not strongly influenced by this uncompensated attraction. This is indeed the case for low TM concentrations $x\leqslant 0.25$.

Direct multi-ion d-d interactions depend strongly on relative angles. Since the d electrons are rather tightly bound to the transition-metal ions, these strong angle-dependent interactions are also short-ranged. The pair potentials alone are thus not expected to reproduce well the total energies in structures with transition-metal near neighbors. For larger TM concentrations certain structural energies are significantly affected by this problem. Section IV D examines their influence in Al-Co compounds at $x=0.2857$.

It is interesting to compare the present GPT potentials for Al-Co with those calculated earlier by Phillips *et al.*[7] The GPT treatment includes a nonlocal pseudopotential, self-consistent electron screening, and direct d-d interactions not considered previously in this context. Phillips *et al.* also carried out their study holding electron density fixed at the value appropriate for FCC aluminum. Here, we consider both a fixed electron density approach, and one of self-consistent variation of electron density with composition and atomic volume. Comparing the potentials quantitatively, the most striking differences is the deep minimum of the Co-Co GPT potential discussed above, which Phillips *et al.* do not observe because of their neglect of direct d-d interactions. Also, the amplitude of the oscillations of the Al-Co and Co-Co GPT potentials is generally larger than in the Phillips *et al.* potentials. This is caused, in part, by the larger effective sp-d hybridization and screening interactions calculated in the first-principles GPT treatment.

The detailed shape of the pair potentials influences mechanical and thermodynamic stability of particular solid structures. Mechanical stability requires that the net force on each atom be small or zero. Thermodynamic stability demands that on average the potential energy per atom be low. These requirements can be met simultaneously by placing atoms in space so that many close interatomic separations are at or near minima of the pair potentials.

Figure 5 shows pair correlation functions of Al_3Ni in the $D0_{11}$ structure. A Gaussian broadening of width 0.15 Å has been applied to mimic typical thermal motion at room temperature. Note the sharp maximum in $g_{AlAl}(r)$ at $r=2.8$ Å, close to where v_2^{AlAl} displays a broad shoulder, and

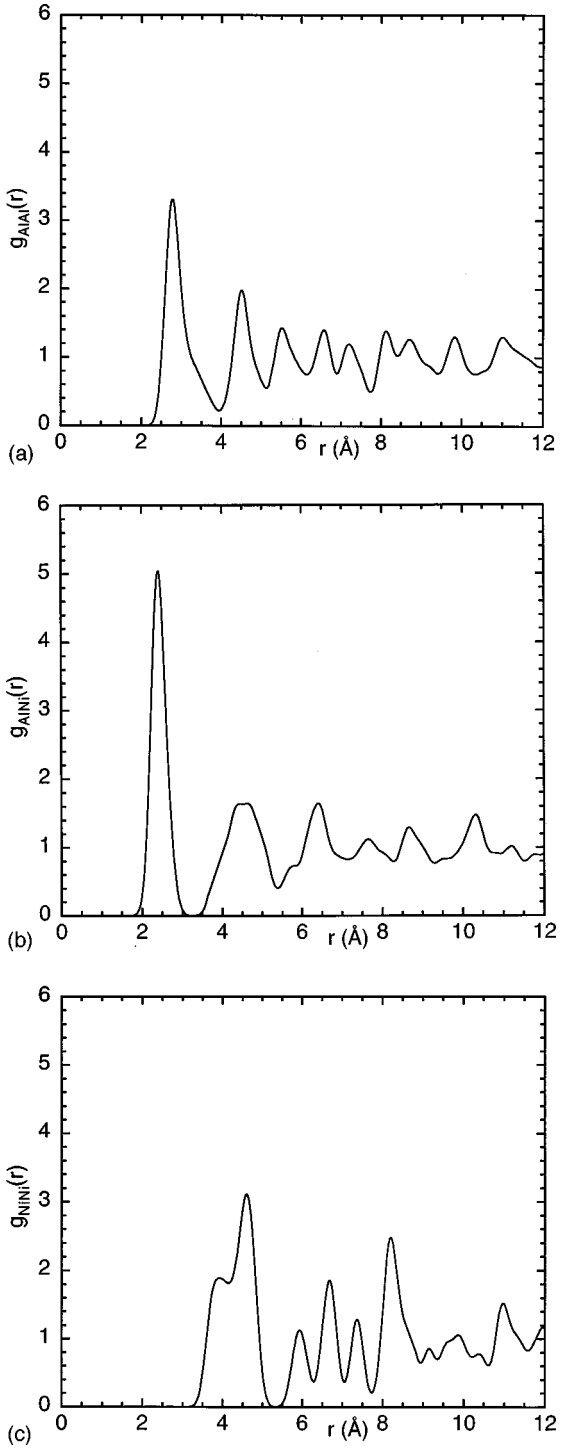

FIG. 5. Pair correlation function for $D0_{11}$ structure of Al_3Ni. (a) $g_{AlAl}(r)$; (b) $g_{AlNi}(r)$; (c) $g_{NiNi}(r)$.

another sharp maximum at $r=4.5$ Å, close to where v_2^{AlAl} has its first minimum. Beyond $r=5$ Å, $g_{\mathrm{AlAl}}(r)$ oscillates rapidly without noticeable relationship to v_2^{AlAl}, which has fallen off to nearly zero. $g_{\mathrm{AlNi}}(r)$ displays pronounced maxima near $r=2.4$, 4.5, 6.4, 8.7, and 10.3 Å. The first three of these peaks lie close to the first three minima of v_2^{AlNi}, while the remaining peaks are slightly to the right of minima of v_2^{AlNi}. Finally, $g_{\mathrm{NiNi}}(r)$ is noteworthy because it vanishes inside the strong first minimum of v_2^{NiNi}. There are no Ni-Ni near neighbors in this structure. However, there is a pronounced double peak at 3.9 and 4.6 Å lying within the second minimum of v_2^{NiNi} and a strong peak 8.2 Å within the fourth minimum of v_2^{NiNi}.

Different structures can produce similar correlation functions, also with peaks fairly close to the pair-potential minima. M- and O-$Al_{13}Co_4$ and Al_3Ni, for example, being approximants to the same 8 Å decagonal phase, possess rather similar correlation functions. Correlation functions for several Al-Co structures have been published previously.[20] These correlation functions also generally show peaks close to the pair-potential minima, explaining why the particular structures are likely to enjoy mechanical and thermodynamic stability. Not surprisingly, both structures have similar mechanical stability and cohesive energy using either the Al-Co or the Al-Ni pair potentials.

IV. CALCULATIONS

This section outlines our study of mechanical and thermodynamic stability of real and hypothetical Al-Co and Al-Ni structures. We evaluate the energy and forces acting on atoms in a wide variety of structures. After relaxing these structures to a state of mechanical equilibrium, we examine net atomic displacements as well as final energies. The atomic displacements indicate the mechanical stability of various structures using our pair potentials. The final relaxed energies indicate the thermodynamic stability (at absolute zero) of the structures.

Thermodynamically stable structures form the convex hull of a graph of free energy versus composition. At low temperatures the free energy reduces to the enthalpy. At low pressure (e.g., one atmosphere), neglect of PV work reduces enthalpy to internal total energy. When comparing total energies, the atomic volume Ω should, in principle, be adjusted to minimize the energy of each structure. As demonstrated in paper I, this is entirely feasible within the GPT method, but it would be unduly laborious here for the large number of structures under consideration. For convenience in the present work, therefore, we have taken atomic volumes from either experiment or, where appropriate, from theoretical considerations.

To calculate total energy, we sum all pairwise interactions up to a cutoff. The cutoff is needed because the slowly decaying Friedel oscillations cause remote atoms to contribute significantly to the total energy. As in paper I, we set the cutoff at $8.25R_{\mathrm{WS}}$, where R_{WS} is the Wigner-Seitz radius corresponding to atomic volume $\Omega=4\pi R_{\mathrm{WS}}^3/3$. In general, defining the cutoff in terms of R_{WS} is advantageous because the set of interactions among atoms remains unchanged as the atomic volume of a structure is varied. The choice 8.25 is somewhat arbitrary, but has been found to be the minimum value that provides adequate convergence. Our relaxation technique employs the IMSL conjugate gradient program ZXCGR. We relax configurations until the average force per atom is less than 10^{-6} eV/Å. Lattice constants are held fixed during relaxation.

To predict the phase diagram requires considering every conceivable structure. The predicted phase diagram is the convex hull of the scatter plot of energy versus concentration. This is clearly an untenable job. Rather, we can consider a limited number of candidate structures. Efficiency

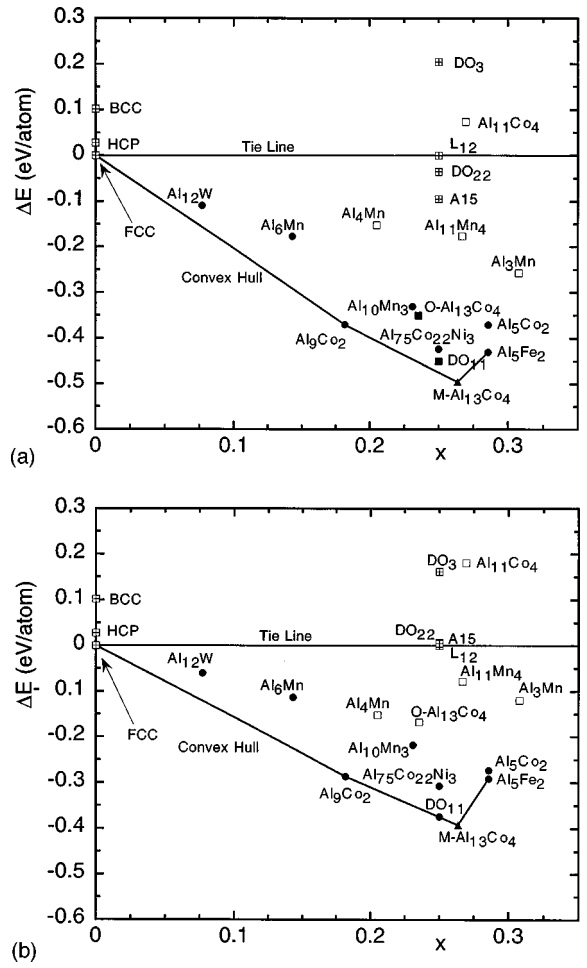

FIG. 6. Scatter plot of structural energies (a) $x=0$ Al-Co potentials and (b) $x=0$ Al-Ni potentials. Plotting symbols indicate displacements under relaxation: unrelaxed symmetric structure (⊞); $\Delta R \leqslant 0.1$ Å (●); 0.1 Å $< \Delta R \leqslant 0.2$ Å (▲); 0.2 Å $< \Delta R \leqslant 0.3$ Å (■); unrelaxed unstable structure (□).

dictates we should consider the most plausible structures, so we draw from existing knowledge[25] of intermetallic structures and consider structures (listed in Table I) which do prove stable for related aluminum-rich transition metal alloys, especially those involving metals such as Cu, Fe or Mn that lie near Co and Ni in the Periodic Table.

A. $x=0$ GPT treatment

Because of the large number of candidate structures at different compositions, we evaluate stability first using the $x=0$ GPT potentials. Later, in Sec. IV C we apply the full GPT to a subset of these structures. With the $x=0$ potentials, we scale the structures isotropically to the hypothetical atomic volume at which the free-electron density matches that of pure FCC aluminum ($0.18076/\text{Å}^3$), as given by Eq. (16) of paper I. To calculate these volumes, we employ the effective valences obtained at $x=0$ in paper I ($Z=3$ for Al, $Z=1.8$ for Co and $Z=1.7326$ for Ni).

Figure 6 displays our $x=0$ results for Al-Co and Al-Ni in scatter plots of relative total energy per atom, $\Delta E = \Delta E_{\text{tot}}/N$, versus x. Here ΔE denotes the difference of relaxed energy from the tie line connecting FCC Al ($x=0$) to Al_3TM in the structure $L1_2$ ($x=0.25$). The data points are labeled with the name of the structure. We replace the transition metal in these structures with Co or Ni. Plotting symbols are used to distinguish degrees of mechanical stability. Highly symmetric structures do not relax because there are no net forces on individual atoms. These are marked with a ⊞ symbol. Some of these structures, $D0_3$ for example, are unstable because small random initial displacements result in large displacements under relaxation away from the symmetric structure. Structures with modest average atomic displacements $\overline{\Delta R}$ are marked with filled shapes (circle, triangle and square for $\overline{\Delta R}$ less than 0.1, 0.2 and 0.3 Å, respectively) at their relaxed energy. Several structures are mechanically unstable ($\overline{\Delta R} \geqslant 0.3$ Å). Their unrelaxed energies are marked with an open square.

Some unstable structures such as Al_4Mn and Al_3Mn are decagonal quasicrystal approximants related in structure to O- and M-$Al_{13}Co_4$ but with a six-layer repeat rather than a four-layer repeat.[19] The proposed structure[16] of $Al_{11}Co_4$ is unstable using our $x=0$ pair potentials, and has a high unrelaxed energy. Our calculation thus supports the identification[11] of $Al_{75}Co_{22}Ni_3$ as the structure better associated with the phase Y-$Al_{13}Co_4$, because of its mechanical stability and low relaxed energy.

A previous problem with $Al_{12}W$ falling below the tie line connecting FCC Al with Al_9Co_2 encountered by Phillips *et al.*[7] has been solved with the present treatment. $Al_{12}W$ now lies above that tie line.

Some features of the phase diagrams are not adequately explained by the $x=0$ GPT results. One problem in the Al-Co phase diagram is the metastability of O-$Al_{13}Co_4$ with respect to the tie line from Al_9Co_2 to M-$Al_{13}Co_4$. Experiments suggest, indeed, that the orthorhombic phase is the true ground state, with the monoclinic phase stabilized only by a small concentration of impurities. However, the issues of partial occupation and Al vacancies appear to be crucial to the outcome. To obtain stability of the orthorhombic phase, we propose to add Al vacancies to the experimentally determined structure. This is discussed in Sec. IV B.

Two additional problems occur in the Al-Ni phase diagram. First, the Al_9Co_2 structure lies below the tie line joining FCC Al with Al_3Ni. Also, we find metastability of Al_3Ni with respect to the tie line joining the Al_9Co_2 structure with the M-$Al_{13}Co_4$ structure. Both of these deficiencies are removed through the full composition-dependent GPT.

The final problem, stability of the Al_5Fe_2 structure over the Al_5Co_2 structure in the Al-Co phase diagram, appears to represent a failure of the 2-body truncation of the total energy expansion, Eq. (2). We show in Sec. IV D how three- and four-body interactions overcome the difficulty. With all these problems resolved, we thereby demonstrate that the GPT adequately reproduces the phase diagrams of Al-Co and Al-Ni up to composition $x=0.3$.

B. Partial occupancy

Many complex intermetallic structures exhibit a concentration of vacancies at certain atomic sites. Among the structures considered here, M-$Al_{13}Co_4$ (both the Cm and the C2/m symmetry models), $Al_{75}Co_{22}Ni_3$ and Al_5Fe_2 are known to have partially occupied sites. Vacancies are found primarily

TABLE II. Energetics for partial occupancy in Al-Co systems near $x=0.25$. Energies ΔE are taken from the FCC-L1$_2$ tie line in units of eV/atom, with ΔR in angstroms. M-$Al_{13}Co_4$ with space group *Cm* is the Hudd and Taylor structure (Ref. 14).

Structure		Full		Partial		Annealed		Relaxed	
Name	Space group	x	ΔE	x	ΔE	x	ΔE	ΔE	ΔR
M-$Al_{13}Co_4$	$C2/m$	0.2353	−0.292	0.2415	−0.339	0.2424	−0.351	−0.391	0.138
M-$Al_{13}Co_4$	Cm	0.2353	−0.263	0.2532	−0.378	0.2526	−0.427	−0.459	0.078
O-$Al_{13}Co_4$	$Pmn2_1$	0.2353	−0.277			0.2500	−0.402	−0.441	0.107
$Al_{75}Co_{22}Ni_3$	$C2/m$	0.2222	+2.431	0.2484	−0.094	0.2500	−0.409	−0.423	0.053
Al_5Fe_2	$Cmcm$	0.2500	+0.106	0.2703	−0.128	0.2857	−0.417	−0.430	0.037

within flat layer aluminum positions that are unusually close (2.4 Å or less) to another aluminum. One related structure, O-$Al_{13}Co_4$, does not have reported fractional occupancy, but the presence of short Al spacings, and the resulting poor mechanical stability and high calculated energies, suggest partial occupancy may be present.

When experimental data is available on partial occupancy, we may use this data to estimate the total energy of a partially occupied structure. Ordinarily, the energy is the sum over pairs of atomic sites i and j of the bond energy $v_2^{\alpha\beta}(R_{ij};\Omega,x)$ between atoms at those sites. To estimate the energy of a partially occupied structure, we simply multiply each bond energy by the product $f_i f_j$ of the site occupancies. Such an approximation becomes exact in the absence of correlations between the occupancies of different sites. Table II shows the dramatic reductions in unrelaxed energy when partial occupancy is incorporated in this manner.

An alternate way to calculate energies in the presence of partial occupancy is to generate specific individual configurations with every site either fully occupied or fully vacant. This approach can incorporate correlations among site occupancy. Because the partial occupancy in Al-Co is often linked with short interatomic distances, we may expect significant correlation between these sites.

A systematic way to generate such configurations is through a fixed site Monte Carlo simulation.[21] We take the experimental structure as a list of possible atomic positions, and populate these sites with a smaller number of atoms. Then, atoms hop among the available sites, with moves accepted or rejected according to the usual Metropolis criterion. At elevated temperatures we can generate occupation statistics for comparison with experimental occupancies. At low temperatures we can generate specific low energy distributions of vacancies among sites. In practice, we perform our simulations holding the cobalt atoms fixed at their experimental positions because there are no reports of fractional occupancy at these sites. Only aluminum atoms are permitted to move. The energies of configurations generated in this way are listed in Table II under the heading ''annealed.'' Compositions x differ slightly between the ''partial'' and ''annealed'' columns because we simulate a single unit cell with an integral number of atoms.

Several features are noteworthy. First of all, when experimental data on partial occupancy is available, we can compare it with the fractional occupancy statistics from Monte Carlo simulation. For this purpose, we perform the simulation at $T=1000$ K, because that is characteristic of typical annealing temperatures. We declare sites with occupancy $f<0.95$ to be partially occupied. The simulated composition is taken as the nearest integer number of aluminums to the reported composition. For M-$Al_{13}Co_4$ with space group C2/m, and for Al_5Fe_2, we find complete agreement in assignment of partially occupied sites. We find substantial, but not perfect, agreement in assignment of partially occupied sites for the Hudd and Taylor[14] structure of M-$Al_{13}Co_4$ with space group Cm. One noteworthy difference is that Hudd and Taylor assign partial occupancy to one puckered layer site, while we find all puckered layer sites are fully occupied. Also, we find low occupancy at Al(7) sites, while Hudd and Taylor report full occupancy.

Full occupancy is claimed[22] for O-$Al_{13}Co_4$. We investigate this claim because of the presence of short (2.24 Å) Al-Al bonds like those related to partial occupancy in M-$Al_{13}Co_4$. The crystallographic structure determination[22] includes Debye-Waller corrections that can mimic partial occupancy. We note substantial correlation between the sites assigned large isotropic thermal displacement coefficients $B_{\rm eq}$ and the low aluminum occupancy sites in a fixed site Monte Carlo simulation. In Fig. 2, circles with solid lines exhibit high Al occupancy ($f\geqslant 0.95$) in our simulations and have small isotropic thermal displacement coefficient ($B_{\rm eq}<1.5$) in the experimental structure. Circles with dashes have large thermal displacements and high simulated Al occupancy. Circles with dots have low simulated occupancy and small thermal displacements. Dashed-dotted circles have large thermal displacements and low occupancy.

Thus, theory and experiment agree that Al atoms are happy to sit at positions in Fig. 2 occupied by solid circles, and agree that atoms do not like to sit at positions occupied by dashed-dotted circles. Overall, the average isotropic thermal displacement coefficient is $B_{\rm eq}=1.2$ for Al atoms and $B_{\rm eq}=0.88$ for Co atoms. Highly occupied Al sites have average $B_{\rm eq}=1.1$. The low occupancy sites have average $B_{\rm eq}=1.7$.

Fractional occupancy solves the problem of mechanical stability of O-$Al_{13}Co_4$. When fully occupied this structure has mean atomic displacement of 0.27 Å, with several Al atom displacements close to 1 Å. We generated a sequence of O-$Al_{13}Co_4$ structures at each integer aluminum composition from 78 to 67 Al atoms per 102-atom unit cell. This covers the composition range from full occupancy down to the lowest suggested composition for M-$Al_{13}Co_4$. We anneal using our fixed site Monte Carlo method from high

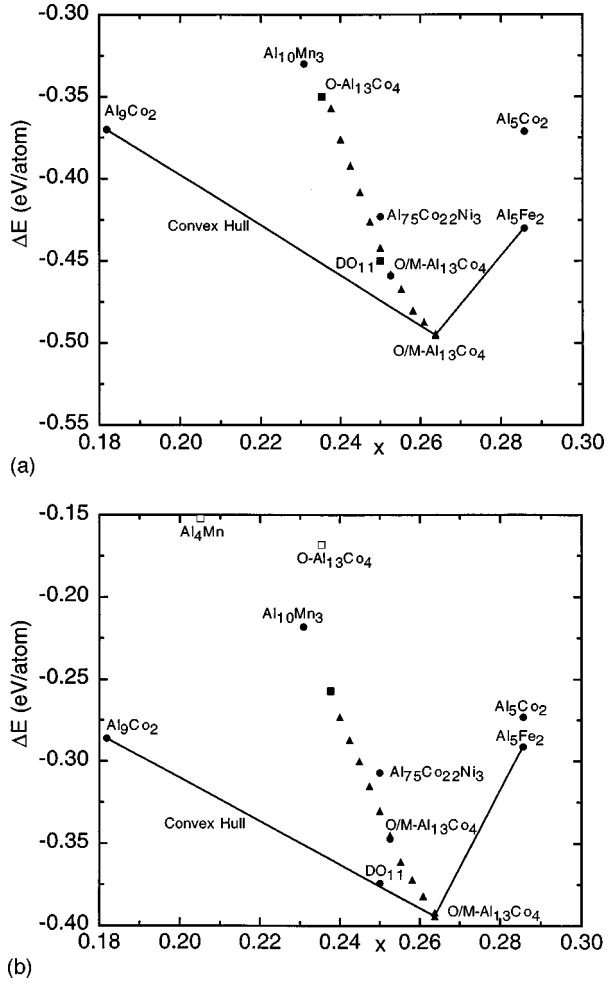

FIG. 7. Closeup of structural energies near $x=0.25$. (a) $x=0$ Al-Co potentials. (b) $x=0$ Al-Ni potentials. Plotting symbols as in Fig. 6.

temperatures down to absolute zero, searching for the lowest energy assignment of Al occupancy. For each aluminum content, we relax the lowest energy annealed configuration and monitor the largest atomic displacements. The largest displacements remain close to 1 Å for 78 through 74 Al/cell. For 73 Al/cell the largest displacement drops below 0.6 Å, and remains small for all Al content through 67 Al/cell.

Relaxed energies for this sequence of annealed structures are plotted in Fig. 7. Note that the total energies fall on the convex hull only at $x=0.2637$, consistent with our suggestion of partial Al occupancy, but far beyond the point ($x=0.2353$) where current phase diagrams place it. The effective negative vacancy formation energy implied here is obtained under the constraints of constant valence electron density and constant $E_{\rm vol}$. These are the same constraints normally applied to the bulk metal and in that case produce a well known virial-pressure contribution to the vacancy formation energy.[26] In bulk Al, this contribution is positive and correctly leads to both a positive vacancy formation energy and, with the present GPT pair potential, a result consistent with experiment as well.[27] A complete treatment of vacancy formation in the alloy also requires inclusion of the composition and atomic volume dependence of the total energy. Section C below includes these effects in our full GPT treatment, and the negative Al vacancy formation energy in O-$Al_{13}Co_4$ remains. It is possible that varying the atomic volume to minimize total energy, and/or including many body interactions, would reduce the value of x at which O-$Al_{13}Co_4$ joins the convex hull. Given the strong instability of the fully occupied structure, however, we believe some Al vacancies are present in O-$Al_{13}Co_4$.

C. Full GPT treatment

Use of $x=0$ GPT potentials was motivated by the near-constancy of the valence electron density observed among the aluminum-rich Al-Co compounds. A more rigorous and accurate approach includes the atomic-volume and composition dependence of each term in the total energy, Eq. (2). In the constant electron-density approximation, the leading volume term $E_{\rm vol}$ has been treated as a constant which does not contribute to energy differences from the tie line. In the full GPT, we must now include $E_{\rm vol}(\Omega,x)$ and also calculate two-body energies using volume- and composition-dependent pair potentials, $v_2^{\alpha\beta}(R_{ij};\Omega,x)$.

Since we consider equilibrium structures, we should, in principle, vary the atomic volume to find the minimum total energy for each candidate structure at fixed x. In practice, we employ experimental atomic volumes where they are known for a given composition, and choose plausible values in cases where experimental atomic volumes are not known. For example, we choose an atomic volume of 108.55 a.u. for Al-Co in the $Al_{12}W$ structure in order to reproduce the electron density of FCC aluminum. For Al-Ni, we let atomic volume vary quadratically with composition to match the electron density of FCC aluminum at $x=0$ and 0.0769 and to match the experimental atomic volume of Al_3Ni at $x=0.25$.

Figure 8 displays the resulting full-GPT structural energies after relaxation for a subset of the structures considered above. The major changes to note occur for Al-Ni, where the observed $D0_{11}$ structure of Al_3Ni achieves thermodynamic stability while Al_9Co_2 loses it. The competing structures O- and M-$Al_{13}Co_4$ lose stability relative to $D0_{11}$ at $x=0.25$. Verifying that the next stable structure of larger x is Al_3Ni_2 would require extending our pair-potential calculations to $x=0.4$, well beyond their intended range of application.

We caution the reader that some calculated energy differences are so small they lie below the expected limits of accuracy of our calculational methods. For example, Al_9Co_2 lies only very slightly (1 meV/atom) above the tie line from FCC Al to $D0_{11}$ using the full-GPT Al-Ni potentials. In principle, we should vary the atomic volumes of both structures to minimize their energies to see if Al_9Co_2 still lies above the convex hull. Many-body interactions or variation of vacancy concentration and unit cell aspect ratio, could easily shift energies sufficiently to move Al_9Co_2 on or off the convex hull.

It is also interesting to compare our calculated energies with other *ab initio* results. Öğüt and Rabe[28] performed electronic structure calculations of total energy for aluminum-rich Al-Co compounds in a variety of structures. Table III compares our results with theirs, and also with similar calculations by Lam and Cohen[29] for pure aluminum. The rather good agreement for pure aluminum validates the GPT approach[30] and indicates the accuracy of truncating Eq. (2) at the two-body term for simple metals. Because of differences

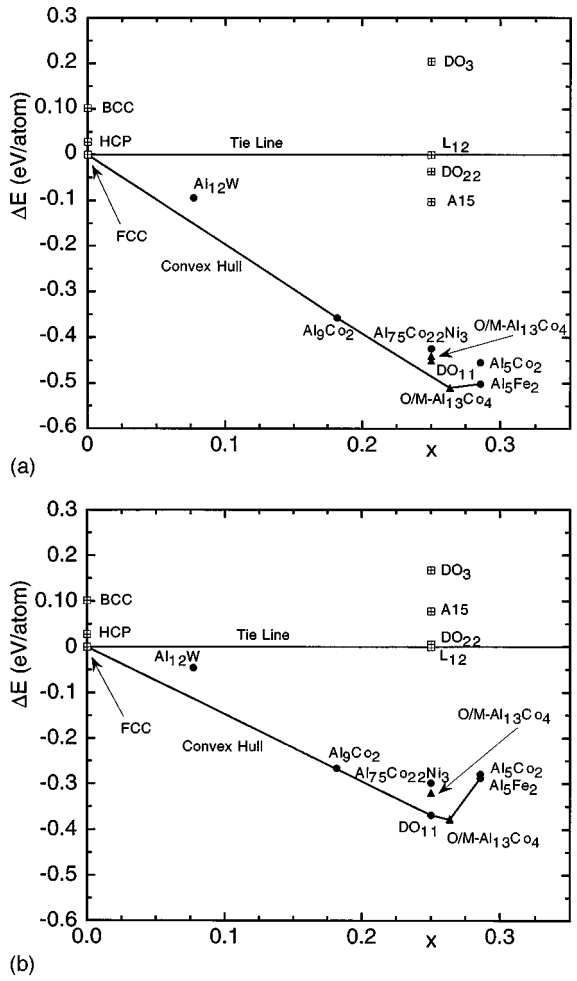

FIG. 8. Scatter plot of structural energies using full volume- and composition-dependent GPT potentials. (a) Al-Co potentials (b) Al-Ni potentials. Plotting symbols as in Fig. 6.

in atomic volume between our Al-Co calculations and Öğüt and Rabe (they scaled to constant electron density assuming a valence $Z=1.5$ for Co) close quantitative agreement is not expected. However, there is agreement in the ordering of energies among structures $D0_3$, $L1_2$, $D0_{22}$ and A15 at $x=0.25$, as well as in the sign and approximate magnitude of ΔE for the $Al_{12}W$ structure. In Table III and in Figs. 6 and 8 we take the ratio $c/a=2.0$ for the $D0_{22}$ structure.

We can further compare calculated formation enthalpies with experiment. Using the full GPT truncated at two-body interactions, we calculate cohesive energies $E_{\rm coh}$ ($E_{\rm tot}/N$ relative to the spin-polarized free atom) of -3.565 eV/atom for FCC aluminum, -6.210 for (nonmagnetic) FCC cobalt, and -5.197 for (nonmagnetic) FCC nickel. We calculate the enthalpy of formation of the aluminum-rich alloys by subtracting their cohesive energies from the tie lines connecting aluminum with cobalt and nickel. Table IV lists experimental[31] and calculated values of

$$\Delta H^{\rm for}=E_{\rm coh}-xE^{\rm Co}_{\rm coh}-(1-x)E^{\rm Al}_{\rm coh}. \qquad (3)$$

This table omits comparison with the reported experimental value for monoclinic $Al_{13}Co_4$ because the reported composition[32] of the experimental sample, $x=0.2253$, falls outside reasonable limits for single phase composition, and

TABLE III. GPT structural energies ΔE for Al and Al-Co compounds compared with other *ab initio* calculations. Energies are with respect to the FCC-$L1_2$ tie line in units of eV/atom.

Structure	x	LC[a]	OR[b]	$x=0$ GPT	full GPT
FCC	0.0000	0	0	0	0
HCP	0.0000	0.033	0.057	0.028	0.028
BCC	0.0000	0.102	0.103	0.102	0.102
$Al_{12}W$	0.0769		−0.044	−0.066	−0.052
$D0_3$	0.2500		0.128	0.205	0.205
$L1_2$	0.2500		0	0	0
$D0_{22}$	0.2500		−0.010	−0.035	−0.036
$A15$	0.2500		−0.083	−0.095	−0.102

[a]Lam and Cohen (Ref. 29).
[b]Öğüt and Rabe (Ref. 28).

the experimental $\Delta H^{\rm for}$ does not lie on the convex hull of reported values. Energies for Al_9Co_2, Al_5Co_2 and Al_3Ni are for relaxed structures at experimental composition and atomic volume. For Al_3Co we use the partially occupied O-$Al_{13}Co_4$ structure at $x=0.25$ and atomic volume 100.0 a.u.

D. Failure of two-body truncation for $x>0.25$

The final difficulty to consider is the lack of stability of the Al_5Co_2 structure compared with the Al_5Fe_2 structure using Al-Co interactions. This is evident in Figs. 6 and 7 using $x=0$ potentials and persists with the full GPT potentials in Fig. 8. To test the volume dependence of the full GPT result, Fig. 9(a) varies the atomic volume Ω away from its experimental value of 92.89 a.u. for the Al_5Co_2 structure to obtain its predicted equilibrium value where $\partial E_{\rm coh}/\partial\Omega=0$. The Al_5Fe_2 structure is still favored at the latter value of 82.34 a.u. For this reason, we are next led to investigate the role of three- and four-body interactions in Eq. (2).

It is reasonable to suppose that many-body interactions are important in these structures because at this high Co concentration ($x=0.2857$) many transition metal atoms are near neighbors of each other. Al_5Co_2 possesses equilateral triangles of Co atoms with edge length 2.912 Å before relaxation. These are on opposite faces of Al_6Co_6 icosahedra surrounding Al(1) atoms. Al_5Fe_2, in contrast, exhibits isosceles triangles of transition metal atoms with edge lengths 2.939, 2.939, and 4.107 Å before relaxation.

Transition metal neighbors can also occur at lower x. For example, in the O-$Al_{13}Co_4$ structure, short 2.86 Å Co separations occur in flat layers. However, these occur only in

TABLE IV. Experimental and calculated enthalpies of formation $\Delta H^{\rm for}$ for observed Al-Co and Al-Ni compounds in units of eV/atom.

Compound	x	$\Delta H^{\rm for}_{\rm expt}$	$\Delta H^{\rm for}_{\rm calc}$
Al	0.0000	0	0
Al_9Co_2	0.1818	−0.31	−0.306
Al_3Co	0.2500	−0.40	−0.402
Al_5Co_2	0.2857	−0.43	−0.374
Al_3Ni	0.2500	−0.40	−0.310

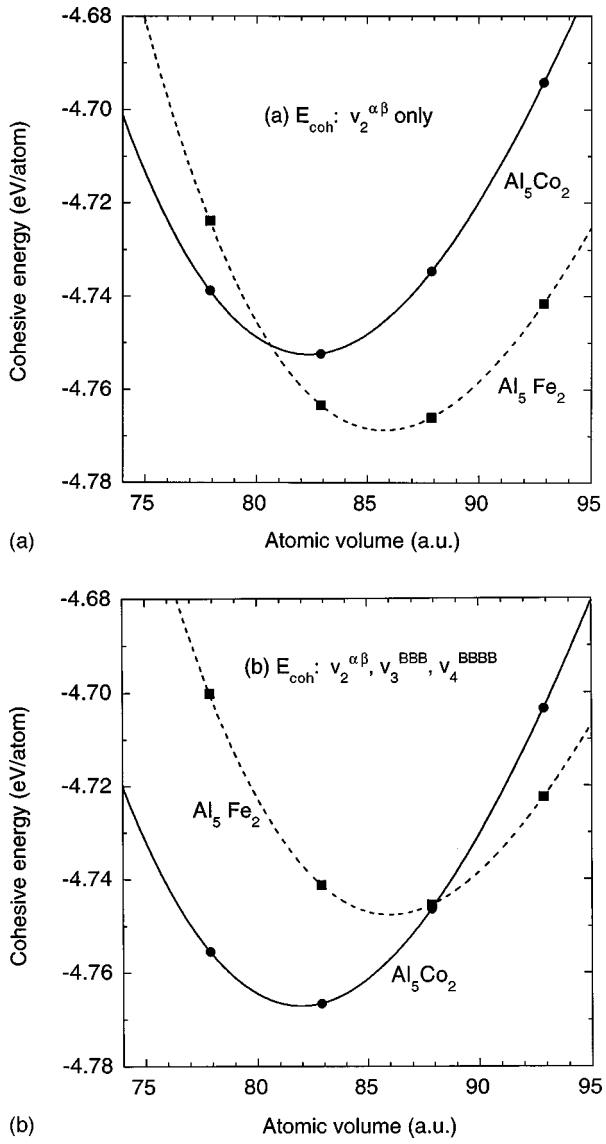

FIG. 9. Volume dependence of the cohesive energy for Al-Co in the structures Al_5Co_2 (solid curves) and Al_5Fe_2 (dashed curves). (a) Pair potentials only, with full relaxation at each volume calculated (solid points). (b) Including three- and four-body Co interactions, in the relaxed configurations of (a).

pairs of transition metal ions, never within triplets. Thus those short Co spacings could contribute to v_3^{ABB} but not to v_3^{BBB}. The inclusion of v_3^{ABB}, etc., may be needed for proper relaxation of the fully occupied O-$Al_{13}Co_4$ structure. With only pair interactions, some Co spacings shrank to the physically unrealistic distance of 1.84 Å during relaxation. This distance is near the strongly negative first minimum of v_2^{CoCo}. Such spacings might be prevented by inclusion of v_3^{ABB}, although the detailed nature of the many-body cross potentials has yet to be investigated. Fortunately, for less than full Al occupancy, such mechanical instability does not occur.

Figure 10 displays the dependence of v_3^{BBB} on distance d and angle θ for isosceles triangles of Co near-neighbor ions. For the triangles present in the two structures under consideration, $d/R_{\mathrm{WS}} \approx 2$. For the equilateral triangles in Al_5Co_2, $\theta = 60°$, while for the isosceles triangles in Al_5Fe_2, θ

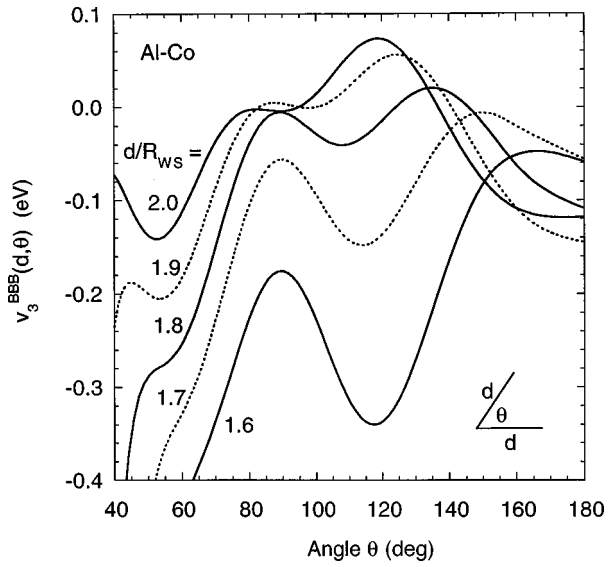

FIG. 10. Three-ion triplet potential $v_3^{BBB}(d,\theta)$ for Co ions in Al-Co compounds at $x = 0.2857$.

$= 88.6°$. Inspecting Fig. 10, we see that the three-body interaction will tend to stabilize the equilateral triangles over the isosceles triangles and hence favor the Al_5Co_2 structure. Interestingly, for pure elemental Fe, the triplet potentials favor the isosceles triangles over the equilateral triangles.[6] If that remains true in the aluminum rich alloy, that would explain formation of the Al_5Fe_2 structure in the Al-Fe binary alloy family.

Because of the long-range sp-d hybridization interaction, the many-body potentials oscillate with non-negligible amplitude out to large distances in a similar manner to the Friedel oscillations in the pair potentials. While the contributions of the near-neighbor triangles described above provide the leading effect, it is necessary here to include both three- and four-body interactions out to the cutoff radius of 8.25 R_{WS}. When this is done and we reexamine the atomic-volume dependence of the cohesive energy, we find that at its predicted equilibrium atomic volume the structure Al_5Co_2 is indeed favored over the structure Al_5Fe_2, as shown in Fig. 9(b). This has resulted primarily from the Al_5Fe_2 cohesion curve being shifted upward in energy with little change in the Al_5Co_2 cohesive properties. The predicted equilibrium atomic volume for Al_5Co_2 is now 81.96 a.u. and the cohesive energy is -4.767 eV/atom. Recalculating the heat of formation yields $\Delta H^{\mathrm{for}} = -0.446$ eV/atom (assuming $E_{\mathrm{coh}}^{\mathrm{Co}}$ and $E_{\mathrm{coh}}^{\mathrm{Al}}$ are unchanged). The bulk modulus is calculated to be 1.16 Mbar.

V. CONCLUSIONS

In conclusion, we have shown that a first-principles multi-ion expansion of the total energy calculated within the generalized pseudopotential theory can faithfully reproduce the aluminum-rich end of the Al-Co and Al-Ni binary phase diagrams. The GPT total energy functional incorporates a full atomic-volume and composition dependence to its volume term and interatomic potentials, while providing a self-consistent treatment of all nearly-free sp electron, sp-d hybridization, and d-d tight-binding contributions. At low transition-metal concentrations, it suffices to truncate the ex-

pansion at two-ion pair potentials. At higher transition-metal concentrations, when transition metal ions have two or more transition-metal near neighbors, three- and four-ion potentials are needed to correctly reproduce the known phase diagram of $Al_{1-x}Co_x$.

To understand stability of certain complex crystal structures related to decagonal quasicrystals, it proves necessary to assume partial occupancy of many aluminum sites. Where experimental data on partial occupancy is available,[14,13] it supports our assignments of partially occupied sites. In the case of O-$Al_{13}Co_4$, we offer our calculations as a suggestion for further experimental study.

The GPT pair potentials utilized in this work may be employed more generally in structural relaxation and phonon studies, and in Monte Carlo or molecular dynamics simulations. They can provide an efficient, but accurate, alternative to other more time consuming and less flexible *ab initio* methods. At high transition-metal concentrations, however, many-body interactions must be considered. These are currently quite time consuming to evaluate from first principles, because the multidimensionality of the potentials has so far required that they be reevaluated each time they are used, as has been done in the present work. The short-range contributions to the three- and four-ion potentials can be analytically modeled and used for simulation applications in some cases such as BCC transition metals.[33] Alternatively, the multi-ion potentials may be approximately folded down and combined with the two-ion potential to form an effective pair potential.[33] This is an especially promising route to solving the difficulty of overbinding of transition-metal near neighbors with the existing pair potentials and could provide an efficient means of extending the present treatment of $Al_{1-x}Co_x$ and $Al_{1-x}Ni_x$ systems to higher x.

The two sets (Al-Co and Al-Ni) of binary alloy pair potentials include five out of the six necessary interactions to describe aluminum-rich Al-Ni-Co ternary compounds. This compound is noteworthy for its thermodynamically stable decagonal quasicrystal phase.[8] We plan to create ternary interactions for this compound in order to create and evaluate atomistic models of the quasicrystalline structure. Similar methods may be employed for Al-Cu-Co, which also boasts a stable decagonal phase,[8] and for Al-Cu-Fe, which exhibits a stable icosahedral quasicrystal phase.[34]

We wish to acknowledge useful discussions with Jun Zou, Rob Phillips, and Eric Cockayne. The first author (M.W.) acknowledges support by the National Science Foundation under Grant No. DMR-9221596. The work of the second author (J.A.M.) was performed under the auspices of the U.S. Department of Energy by the Lawrence Livermore National Laboratory under Contract No. W-7405-ENG-48.

[1] *Intermetallic Compounds: Principles and Practice*, edited by J. H. Westbrook and R. L. Fleischer (Wiley, New York, 1995).

[2] M. M. Schwartz, *Emerging Engineering Materials* (Technomic, Lancaster, PA, 1996).

[3] D. P. Shoemaker and C. B. Shoemaker, in *Introduction to Quasicrystals*, edited by M. V. Jaric (Academic, San Diego, 1988), p. 1.

[4] For reviews of topics in the field of quasicrystals, see *Quasicrystals: The State of the Art*, edited by D. P. DiVincenzo and P. J. Steinhardt (World Scientific, Singapore, 1991), and C. Janot, *Quasicrystals: A Primer* (Oxford University, New York, 1992).

[5] J. A. Moriarty and M. Widom, Phys. Rev. B **56**, 7905 (1997).

[6] J. A. Moriarty, Phys. Rev. B **38**, 3199 (1988).

[7] R. Phillips, J. Zou, A. E. Carlsson, and M. Widom, Phys. Rev. B **49**, 9322 (1994). A related set of pair potentials for Al-Mn alloys is described in Ref. 37.

[8] A. P. Tsai, A. Inoue, and T. Matsumoto, Mater. Trans., JIM **30**, 463 (1989).

[9] A. J. McAlister, Bull. Alloy Phase Diagrams **10**, 646 (1989).

[10] H. Okamoto, J. Phase Equilib. **14**, 257 (1993).

[11] B. Grushko, R. Wittenberg, K. Bickmann, and C. Freiburg, in *Proceedings of the Fifth International Conference on Quasicrystals*, edited by C. Janot and R. Mosseri (World Scientific, Singapore, 1995), p. 684; B. Grushko, R. Wittenberg, K. Bickmann, and C. Freiburg, J. Alloys Compd. **233**, 279 (1996).

[12] H. Okamoto and T. B. Massalski, J. Phase Equilib. **14**, 316 (1993).

[13] C. Freiburg, B. Grushko, R. Wittenberg, and W. Reichert, Mater. Sci. Forum **228-231**, 583 (1996).

[14] R. C. Hudd and W. H. Taylor, Acta Crystallogr. **15**, 441 (1962).

[15] B. Zhang, V. Gramlich, and W. Steurer, Z. Kristallogr. **210**, 498 (1995).

[16] X. Z. Li, N. C. Shi, Z. S. Ma, X. L. Ma, and K. H. Kuo, Philos. Mag. Lett. **72**, 79 (1995).

[17] X. L. Ma, X. Z. Li, and K. H. Kuo, Acta Crystallogr., Sect. B: Struct. Sci. **51**, 36 (1995).

[18] X. L. Ma and K. H. Kuo, Metall. Trans. A **23**, 1121 (1992).

[19] C. L. Henley, J. Non-Cryst. Solids **153&154**, 172 (1993).

[20] M. Widom and E. Cockayne, Physica A **232**, 713 (1996).

[21] E. Cockayne and M. Widom, Philos. Mag. A **77**, 593 (1998).

[22] J. Grin, U. Burkhardt, M. Ellner, and K. Peters, J. Alloys Compd. **206**, 243 (1994).

[23] X. Z. Li, X. L. Ma, and K. H. Kuo, Philos. Mag. Lett. **70**, 221 (1994).

[24] M. Widom, R. Phillips, J. Zou, and A. E. Carlsson, Philos. Mag. B **71**, 397 (1995).

[25] P. Villars and L. D. Calvert, *Pearson's Handbook of Crystallographic Data for Intermetallic Phases* (American Society for Metals, Materials Park, OH, 1991).

[26] G. Jacucci and R. Taylor, J. Phys. F **9**, 1489 (1979).

[27] J. A. Moriarty (unpublished).

[28] S. Öğüt and K. M. Rabe, Phys. Rev. B **50**, 2075 (1994).

[29] P. K. Lam and M. L. Cohen, Phys. Rev. B **24**, 4224 (1981).

[30] J. A. Moriarty and A. K. McMahan, Phys. Rev. Lett. **48**, 809 (1982); A. K. McMahan and J. A. Moriarty, Phys. Rev. B **27**, 3235 (1983).

[31] F. R. de Boer, R. Boom, W. C. M. Mattens, A. R. Miedema, and A. K. Niessen, *Cohesion in Metals: Transition Metal Alloys* (Elsevier, Amsterdam, 1988), p. 273.

[32] R. Hultgren, P. D. Desai, D. T. Hawkins, M. Gleiser, and K. K. Kelly, *Selected values of Thermodynamic Properties of Binary*

Alloys (American Society of Metals, Materials Park, OH, 1973).
[33] J. A. Moriarty, Phys. Rev. B **42**, 1609 (1990); **49**, 12 431 (1994).
[34] A. P. Tsai, A. Inoue, and T. Masumoto, Jpn. J. Appl. Phys., Part 2 **26**, L1505 (1987).
[35] X. Z. Li, D. Shi, and K. H. Kuo, Philos. Mag. B **66**, 331 (1992).
[36] X. Z. Li and K. H. Kuo, Philos. Mag. B **65**, 525 (1992).
[37] M. Mihalkovic, W.-J. Zhu, C. L. Henley, and R. Phillips, Phys. Rev. B **53**, 9021 (1996).